Journal of Coordination Chemistry

ISSN: 0095-8972 (Print) 1029-0389 (Online) Journal homepage: http://www.tandfonline.com/loi/gcoo20

POM-assisted synthesis of the first cyclohexanediamine-based Salen-type Mn^{III}-dimer complexes

Qiong Wu, Qing Pu, Yongmei Wu, Hongjuan Shi, Yanfang He, Jun Li & Quanshui Fan

To cite this article: Qiong Wu, Qing Pu, Yongmei Wu, Hongjuan Shi, Yanfang He, Jun Li & Quanshui Fan (2015) POM-assisted synthesis of the first cyclohexanediamine-based Salen-type Mn^{III}-dimer complexes, Journal of Coordination Chemistry, 68:6, 1010-1020, DOI: 10.1080/00958972.2015.1006211

To link to this article: http://dx.doi.org/10.1080/00958972.2015.1006211

Journal of Coordination Chemistry, 2015
Vol. 68, No. 6, 1010–1020, http://dx.doi.org/10.1080/00958972.2015.1006211

POM-assisted synthesis of the first cyclohexanediamine-based Salen-type Mn^{III}-dimer complexes

QIONG WU†‡*, QING PU†, YONGMEI WU§, HONGJUAN SHI†, YANFANG HE†, JUN LI¶ and QUANSHUI FAN‡*

†Department of Chemical Science and Technology, Kunming University, Kunming, PR China
‡Center for Disease Control and Prevention, Chengdu Military Region, Kunming, PR China
§School of International Cultures and Education, Yunnan University of Finance and Economics, Kunming, PR China
¶Medical School, Kunming University, Kunming, PR China

(*Received 27 August 2014; accepted 30 December 2014*)

The reaction between manganese nitrate and *N,N′*-(±)-ethylene-bis(salicylicyclohexanediaminate) ((±)-salcy) in dilute lacunary polyoxoanion $[PW_9O_{34}]^{9-}$ solution led to isolation of a new Mn-dimer, $[Mn((\pm)\text{-salcy})(N_3)]_2$ (**1**). Structural analysis indicates that **1** represents the first salcy-based Mn-dimer complex. Magnetic susceptibility studies reveal that **1** shows single-molecule magnet (SMM) behavior from 2 to 5 K.

Keywords: Schiff base; Manganese; POM solution; Magnetic properties

1. Introduction

In the past two decade, an enormous amount of research has been devoted to the design and synthesis of molecular-based magnetic materials due to their potential applications in

*Corresponding authors. Email: wuqiongkm@163.com (Q. Wu); fqs168@126.com (Q. Fan)

computer molecular devices and high-density information storage [1, 2]. A variety of related compounds have been synthesized and investigated with trivalent manganese ion (Mn^{III}) owing to the large ground spin number and obvious Jahn–Teller effects [3]. On the other hand, ideal ligands should not only have the potential to stabilize the coordination environment of a metal center, but also have controllable structures to manipulate the reactivity or magnetic behaviors for different applications [4–7]. Therefore, tetradentate Schiff base ligands (salen) and its analogs have been widely used as important ligands to elaborate various magnetic materials. Therefore, in the last few years, the family of manganese–salen-type Schiff base compounds has become one of the most appealing candidates for construction of molecular-based magnetic materials [8–11].

It's worth noting that in the solution the steric characteristics of Schiff base ligands can lead to two different structures of cationic Mn^{III}– salen complexes, monomer or out-of-plane dimer configuration; different reaction conditions could result in interconversion in solid forms [12]. However, the relationship between conditions and isolated forms is not understood.

Up to present, almost of the out-of-plane dimer motif constructed by commonly used Schiff-base ligand have been isolated (see scheme 1), including $[Mn^{III}(salen)(H_2O)]_2$ (salen = *N,N′*-ethylene-bis(salicylideneiminate)) [13], $[Mn^{III}(salpn)(H_2O)]_2$, $[Mn^{III}(salphen)(Py)]_2$ (salphen = *N,N′*-(1,3propylene)bis(salicylideneiminate)) [14], $[Mn^{III}(salmen)(N_3)(H_2O)]_2$ (salmen = *N,N′*-(1methylethylene)bis(salicylideneiminate)) [15, 16], $[Mn^{III}(saldmen)(H_2O)]_2$ (saldmen = *N,N′*(1,1-dimethylethylene)bis(salicylideneiminate)) [17], and $[Mn^{III}(saltmen)(ReO_4)(H_2O)]_2$ (saltmen = *N,N′*-ethylene-bis(salicylideneiminate)) [18]. However, probably due to the relatively larger repulsion between monomers, cyclohexanediamine-based manganese-dimers still have not been obtained, being the last piece to the puzzle of the 'manganese-dimer Schiff-base family.' Whereas, the challenge of preparing salcy-based Mn-dimer complexes remains a rewarding research area, since the Mn–salen family is well researched a class of well research complexes, systematically explore the relationship between reaction conditions and complexes configuration may provide some clues for further understanding the formation mechanisms of complexes.

A recent achievements in this field has focused on the introduction of saturated polyoxometalates (POMs) into Mn–salen system as a promising method for producing new organic–inorganic magnetic materials [19–24]. As an extension of previous work, we tried to use diluted lacunary POM solution as the reaction medium, to further explore the POM's template effect for Mn–Schiff base complexes. Hence, in the present work, we chose manganese nitrate and salcy as starting materials with β-$Na_8[HPW_9O_{34}]\cdot 24H_2O$ solution as reaction medium for our synthetic strategy, and synthesized the first example of cyclohexanediamine-based Mn-dimer complex $[Mn((\pm)\text{-salcy})(N_3)]_2$ (**1**). The magnetic properties of **1** were also investigated. Under identical reaction environment when we used pure aqueous solution as reaction medium the mononuclear $[Mn((\pm)\text{-salcy})(N_3)(H_2O)]\cdot H_2O$ (**2**) was obtained (see scheme 2).

2. Experimental

2.1. *Materials and methods*

All chemicals were purchased from Aladdin and used without purification. Elemental analyses (C, H, and N) were performed on a Perkin–Elmer 2400 CHN elemental analyzer. Manganese was determined by a Leaman inductively coupled plasma (ICP) spectrometer.

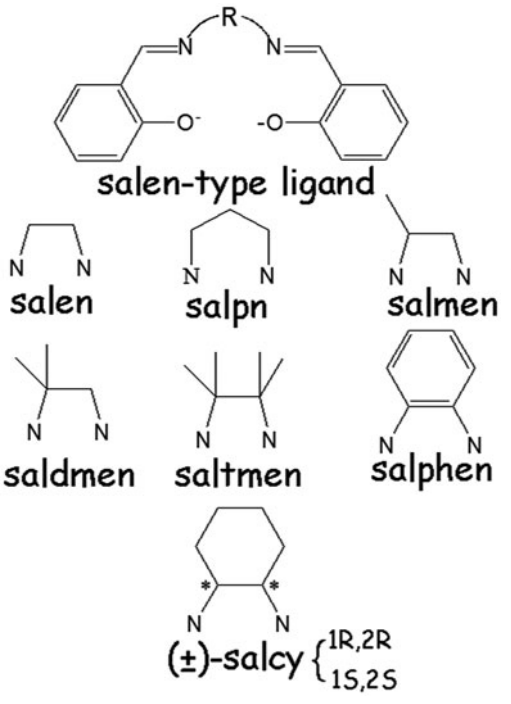

Scheme 1. Schematic view of commonly used Schiff base ligands.

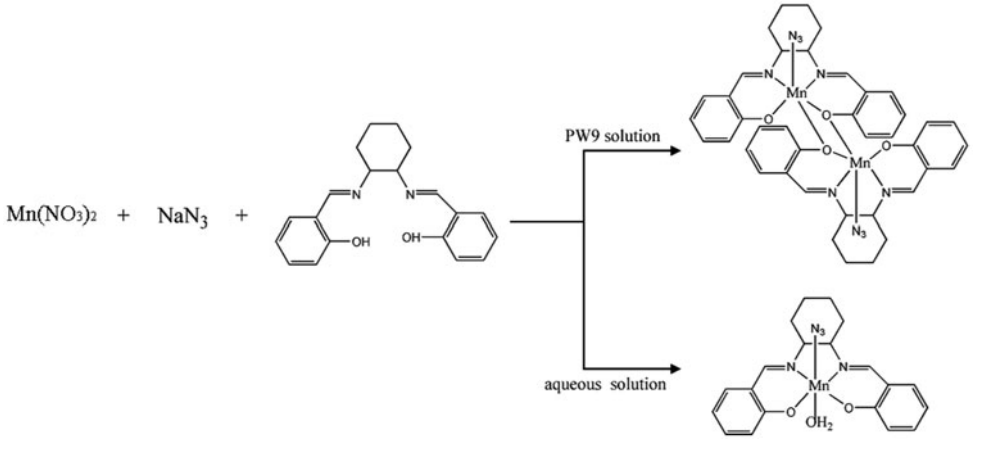

Scheme 2. Schematic view of the synthetic route for **1** and **2**.

IR spectra were recorded from 400 to 4000 cm^{-1} on an Alpha Centaurt FTIR spectrophotometer with pressed KBr pellets. XPS analyses were performed on a VG ESCALABMKII spectrometer with an Mg–*K*α (1253.6 eV) achromatic X-ray source. The vacuum inside the analysis chamber was maintained at 6.2×10^{-6} Pa during the analysis. The variable-temperature solid-state magnetic susceptibilities (χ_M) were measured with a Quantum Design

Table 1. Crystal data and structure refinement for **1** and **2**.

	1	**2**
Empirical formula	$C_{40}H_{40}N_{10}O_4Mn_2$	$C_{20}H_{24}N_5O_3Mn$
Formula weight	834.7	433.3
Temperature (K)	296(2)	296(2)
Wavelength (Å)	0.71073	0.71073
Crystal system	Monoclinic	Triclinic
Space group	*P*21/*c*	*P*-1
a (Å)	8.859(5)	8.1460(16)
b (Å)	14.496(8)	11.250(2)
c (Å)	14.722(9)	12.488(3)
α (°)		115.896(2)
β (°)	103.156(11)	92.080(3)
γ (°)		99.729(3)
Volume (Å^3)	1841.0(18)	1006.9(4)
Z	2	2
Density (calculated)	1.506	1.429
Absorption coefficient	0.744	0.687
F(0 0 0)	864	448
Reflections collected/unique	8446/3075 [*R*(int) = 0.1150]	7994/3526 [*R*(int) = 0.0561]
Data/restraints/parameters	3075/0/248	3526/0/266
Goodness-of-fit on F^2	1.041	1.006
Final *R* indices [$I > 2\sigma(I)$] *R* indices (all data)	$R_1 = 0.0792$, $wR_2 = 0.1930$	$R_1 = 0.0606$, $wR_2 = 0.1643$
Largest diff. peak and hole	0.589 and −0.552 e Å^{-3}	0.505 and −0.465 e Å^{-3}

[a] $R_1 = \Sigma||F_o| - |F_c||/\Sigma|F_o|$.
[b] $wR_2 = \Sigma[w(F_o^2 - F_c^2)^2]/\Sigma[w(F_o^2)^2]^{1/2}$.

Table 2. Selected bond lengths (Å) and angles (°) of **1**.

Mn(1)–O(6)	1.867(4)	O(5)–C(34)	1.337(8)
Mn(1)–O(5)	1.920(4)	O(6)–C(9)	1.334(7)
Mn(1)–N(6)	1.981(6)	N(5)–C(19)	1.234(9)
Mn(1)–N(5)	1.999(5)	N(5)–C(81)	1.508(10)
Mn(1)–N(1)	2.118(6)	N(6)–C(18)	1.290(9)
O(6)–Mn(1)–O(5)	92.08(18)	N(5)–Mn(1)–N(1)	92.3(2)
O(6)–Mn(1)–N(6)	92.3(2)	N(6)–Mn(1)–N(5)	81.8(2)
O(5)–Mn(1)–N(6)	162.7(2)	O(6)–Mn(1)–N(1)	99.4(2)
O(6)–Mn(1)–N(5)	167.7(2)	O(5)–Mn(1)–N(1)	95.9(2)
O(5)–Mn(1)–N(5)	90.6(2)	N(6)–Mn(1)–N(1)	100.0(3)

Table 3. Selected bond lengths (Å) and angles (°) of **2**.

Mn(2)–O(1)	1.864(3)	O(2)–C(8)	1.327(6)
Mn(2)–O(2)	1.869(3)	N(1)–C(37)	1.296(6)
Mn(2)–N(2)	1.981(4)	N(1)–C(1)	1.483(6)
Mn(2)–N(1)	1.982(4)	N(2)–C(36)	1.291(6)
Mn(2)–N(3)	2.267(4)	N(2)–C(2)	1.483(6)
Mn(2)–O(6)	2.342(3)	N(3)–N(4)	1.181(6)
O(1)–Mn(2)–O(2)	91.72(14)	O(2)–Mn(2)–N(3)	94.85(16)
O(1)–Mn(2)–N(2)	175.42(15)	N(2)–Mn(2)–N(3)	86.89(15)
O(2)–Mn(2)–N(2)	92.83(15)	N(1)–Mn(2)–N(3)	89.77(16)
O(1)–Mn(2)–N(1)	92.65(15)	O(1)–Mn(2)–O(6)	91.86(14)
O(2)–Mn(2)–N(1)	173.45(15)	O(2)–Mn(2)–O(6)	90.02(14)
N(2)–Mn(2)–N(1)	82.77(16)	N(2)–Mn(2)–O(6)	87.56(14)
O(1)–Mn(2)–N(3)	93.30(15)	N(1)–Mn(2)–O(6)	84.97(14)

MPMS7 SQUID magnetometer at 0.1 T dc field from 2 to 300 K. Diamagnetic corrections were made with Pascal's constants.

2.2. *Preparation*

2.2.1. Synthesis of the Schiff base ligand. According to classical organic synthesis of Schiff bases [25], salicylaldehyde (0.244 g, 1.0 mM) and (±)-1.2-cyclohexanediamine (0.114 g, 1.0 mM) were dissolved in methanol (25 mL) and the yellow suspension was then refluxed for 4 h under stirring. After cooling the solution on crushed ice, orange–yellow crystals slowly appear (Yield: 72%).

2.2.2. Synthesis of $[Mn((\pm)\text{-salcy})(N_3)]_2$ (1). β-Na_8 $[HPW_9O_{34}]\cdot 24H_2O$ (0.0212 g, 0.01 mM) was dissolved in 30 ml aqueous solution and 5 ml methanol solution containing freshly prepared salcy (0.316 g, 1 mM), 0.251 g (0.1) $Mn(NO_3)_2\cdot 4H_2O$, and 0.065 (0.01 mM) NaN_3 was successively added to above solution. After stirring overnight at room temperature, the obtained brown filtrate was then sealed with parafilm. Dark brown crystals of **1** were isolated after 2 weeks in 42% yield by filtration, washed with methanol, and dried in air. Anal. $C_{40}H_{40}N_{10}O_4Mn_2$ (M_r = 834.7) **1** (%): Calcd C, 57.78; N, 16.68; Mn, 13.13. Found: C, 57.65; N, 16.69; Mn, 13.39.

2.2.3. Synthesis of $[Mn((\pm)\text{-salcy})(N_3)(H_2O)]\cdot H_2O$ (2). Complex **2** was prepared with the same method except that pure aqueous solution was used as the reaction medium and the yield of crystals of **2** is 45%. Anal. $C_{20}H_{24}N_5O_4Mn$ (M_r = 453.3) **2** (%): Calcd C, 54.92; N, 16.01; Mn, 12.56. Found: C, 55.72; N, 16.12; Mn, 12.23.

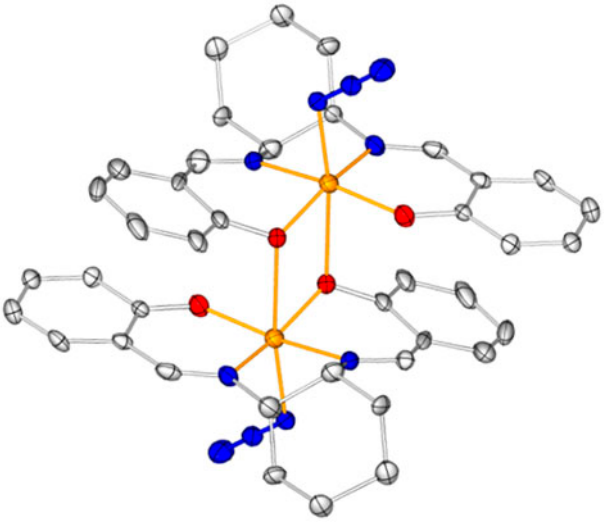

Figure 1. Ball-and-stick view of **1**.

2.3. *X-ray crystallography*

The crystallographic data were collected at 150 K on a Bruker D8 SMART APEX II CCD diffractometer with kappa geometry and Mo–Kα radiation (λ = 0.71073 Å). Suitable crystals were mounted in a thin glass tube and transferred to the goniostat. Multi-scan absorption correction was applied. Data integration was performed using SAINT. Routine Lorentz and polarization corrections were applied. Multi-scan absorption corrections were performed using SADABS [26]. Manganese ions were located by direct methods and successive Fourier syntheses revealed the remaining atoms. Refinements were fully refined by the full-matrix method on F^2 using the SHELXTL-97 crystallographic software package [27]. In the final refinement, all the non-H atoms were anisotropically refined. Hydrogens on carbons of Schiff base ligands were fixed in calculated positions. Hydrogens on methanol cannot be determined from the difference Fourier maps and were directly included in the final molecular formula. The highest residual peak and the deepest hole are 0.725, –0.773, 0.505, and –0.465 e Å^{-3} for **1** and **2**, respectively. The detailed crystal data and structure refinement for **1** and **2** are given in table 1. Selected bond lengths and angles of **1** and **2** are listed in tables 2 and 3, respectively.

3. Results and discussion

3.1. *Synthesis*

The reaction of POMs with Mn–Schiff base complexes has proved an effective route for preparation of new organic–inorganic aggregates. In this field, we have used diamagnetic polyoxometalate (POM) clusters to react with Mn^{III}_2–Schiff base precursors and firstly extracted complexes' intrinsic magnetic behavior in pure inorganic matrix [23]; to improve the activity, we used the *in situ* method to directly react ammonium metavanadate in Mn–Schiff base complex solutions and isolated the {metal–Schiff base}-decorated POM hybrid, in which Mn–Schiff base complexes are templates for formation of V6. As an extension of our research, herein, we tried to adopt opposite strategies, in which POM solution acts as reaction medium to isolate Mn–salen complexes.

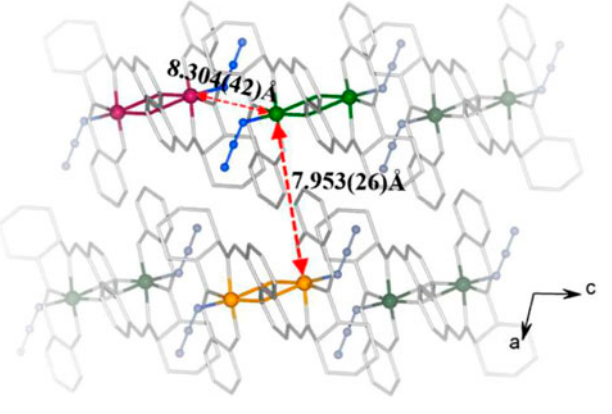

Figure 2. Packing arrangement of **1** viewed along the *b* axis.

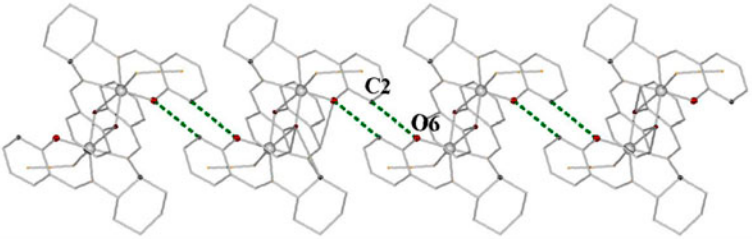

Figure 3. View of the H-bonding interactions among Mn-dimers. The detailed H-bonds are as follows: C2···O6, 3.300(8) Å, C2-H2A, 0.93Å, H2A···O6 2.54 Å, and bond angle C2-H2A···O6 139°.

Table 4. Selected H-Bonds in the crystal structure of **1**.

X	Y	X–H	H···X	X···Y
C(2)	O(6)	0.93	2.54	3.300(8)
C(3)	O(5)	0.93	3.02	3.707(8)
C(3)	O(6)	0.93	2.59	3.823(8)
C(13)	C(3)	0.98	2.85	3.721(1)

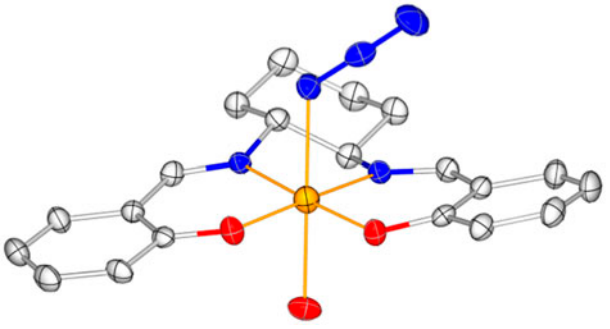

Figure 4. Ball-and-stick view of **2**; solvent waters are omitted for clarity.

Although POM did not cocrystallize with Mn–salcy, in the absence of POM, the isolated Mn–salcy complex was mononuclear. Therefore, we speculate that lacunary POMs offer a specific ion environment that favors dimeric Mn–salcy. Moreover, the use of NaN_3 was also necessary for this reaction system, without it, merely irregular shaped crystalline-like aggregation can be obtained.

3.2. *Crystal structures*

Compound **1** crystallizes in monoclinic *P*21/*c*. As shown in figures 1 and S1 (see online supplemental material at http://dx.doi.org/10.1080/00958972.2015.1006211), the asymmetric unit of **1** contains one R,R–salcy ligand, one manganese ion and one azide unit, in which manganese is five-coordinate with a phenoxo bridge from the other half of enantiomeric S, S–salcy ligand, and resulting in an overall centrosymmetric structure.

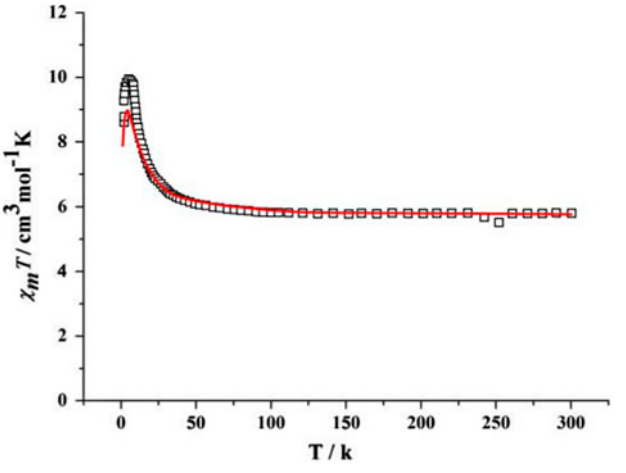

Figure 5. The temperature dependence of the magnetic susceptibility χ. The red lines represent the best fit using an isotropic Heisenberg $S_{Mn} = 2$ dimer model (see http://dx.doi.org/10.1080/00958972.2015.1006211 for color version).

Each Mn^{III} is chelated by the tetradentate Schiff base ligand via N2O2 in the equatorial plane, with Mn–O(N) bond lengths of 1.867(6)–1.999(5) Å, while O(N)–Mn–O bond angles vary from 81.8(2) to 167.7(2)°. The O2N2 donors are nearly coplanar, whereas manganese deviates slightly from the plane. In the apical position, Mn^{III} is coordinated with one azide and one oxygen from neighboring phenoxo. The Mn–O and Mn–N bond lengths are 2.679(5) and 2.117(6) Å, respectively. Two planes of intramolecular Schiff base ligands are nearly parallel to each other. As usually observed for octahedral Mn^{III} ions, Jahn–Teller distortion at the high-spin d4 metal center leads to elongated axis which is nearly perpendicular to the equatorial coordination plane. The oxidation state of Mn can be assigned as Mn^{III} based on the charge–balance consideration, bond–valence sum calculations, and the presence on Mn centers of Jahn–Teller elongation axes.

In the packing arrangement, there are no π–π interactions in **1**; H-bonding connects adjacent $\{Mn_2\}$ moieties into a 1-D supramolecular chain (figure 2). All adjacent $\{Mn_2\}$ complexes possess the identical easy-axis direction, and the shortest intramolecular Mn···Mn distance is 8.302(4) and 7.953(3) Å, respectively (see figures 3 and S3). Typical H-bonds of **1** are listed in table 4.

Compound **2** crystallizes in the triclinic space group *P*-1. As shown in figure S4, the unit cell of **2** is constructed by two racemic-neutral monomeric $[Mn((+)\text{-salcy})(N_3)(H_2O)]$ and $[Mn((-)\text{-salcy})(N_3)(H_2O)]$, and overall exhibiting centrosymmetric configuration. The Mn^{III} in **2** has almost identical coordination geometry with **1** (as depicted in figure 4) except that one apical site is occupied by water, while in **1** a neighboring phenoxo oxygen. The nearest intermolecular Mn···Mn distance is 5.07(15) Å (see figure S5).

3.3. *XPS*

The oxidation states of Mn in **1** are further confirmed by XPS measurement. The XPS spectra were carried out in the energy region of Mn $2p_{3/2}$. The peak at 641.3 eV is ascribed to Mn^{3+} ion (see figure S6). The peak distance between $2p_{3/2}$ and $2p_{1/2}$ is 11.3 eV for Mn^{3+},

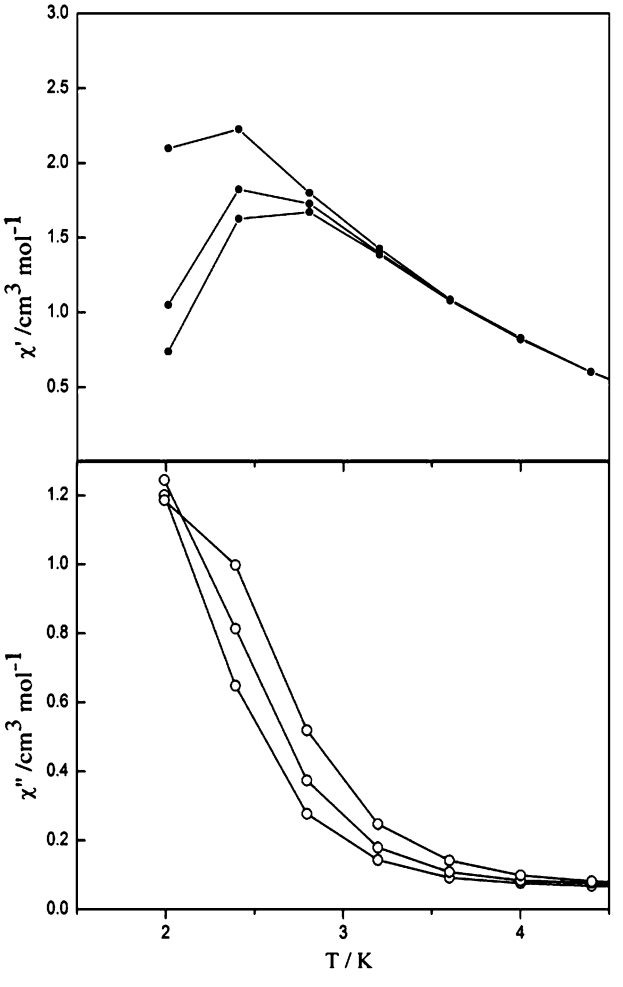

Figure 6. Temperature dependence of the real (χ') and imaginary (χ'') parts of the ac susceptibility for **1** at different ac frequencies under 0.1 T dc field. The ac field fluctuates at a frequency of 100, 400, and 800 Hz, respectively. Solid lines are guides for the eyes.

in agreement with reported results. The XPS result is in accord with the BVS calculations, further confirming the oxidation state Mn^{3+} in **1** and **2**.

3.4. *Magnetic properties for 1 and 2*

The magnetic susceptibilities of **1** were measured with polycrystalline samples at 0.1 T from 2 to 300 K. The thermal variation of the χT product of **1** is shown in figure 5. At 300 K, χT product is 5.96 cm^3 K M^{-1} which is slightly smaller than two high-spin Mn^{III} ($S = 2$). When the temperature was lowered, the χT value increases continuously to a maximum $\chi_m T$ of 9.87 cm^3 K M^{-1} indicating a typical ferromagnetic coupling between Mn^{III} ions, however, further cooling leads to a rapid decrease to 8.3 cm^3 K M^{-1} which is attributed to the presence of zero-field splitting effects of the single Mn^{III} ion and/or weak antiferromagnetic interaction between Mn-dimers.

Considering long interdimer Mn···Mn distance of **1**, the interdimer magnetic interactions that could influence magnetic coupling were neglected [28]. Therefore, the susceptibility data are modeled by the Hamiltonian, given in equation (1) ($S_1 = S_2 = S_{Mn}$, *Siz* is the *z* component of the S*i* operator), in which *J* is the intramolecular magnetic coupling constant between two Mn^{III} ions, *D* is the uniaxial anisotropy of single Mn^{III} ion, and *g* is the *g* tensor:

$$H = g \cdot \beta(S_1 + S_2)H - 2JS_1 \cdot S_2 + D(S_{z1}^2 + S_{z2}^2) \quad (1)$$

The dc susceptibility was simulated using the MAGPACK program (the solid lines in figure 6) [29]. In **1**, single-ion zero-field splitting parameter *D* for two centrosymmetrically related Mn^{III} ions in the dimer are identical, therefore, the best fitting results between the calculated and experimental data of the susceptibility were found with $D = -1.27\ cm^{-1}$. This is consistent with the typical value of –0.38 to 2.53 cm^{-1} for Mn dimer analogs. The interatomic interaction parameter $J = 0.51\ cm^{-1}$ confirms the ferromagnetic interaction between Mn^{III} ions, and the values are close to those of reported ferromagnetic Mn^{III}-dimers.

For evaluating whether **1** possesses single-molecular magnetic (SMM) behavior [16], the temperature and frequency dependence of the ac susceptibility measurement has been carried out at 2–5 K at three different frequencies. The frequency dependent in-phase χ' and out-of-phase χ'' signals suggest SMM behavior for **1** (figure 6). Since the above results agree with previously reported phenoxo-bridged out-of-plane Mn^{III}-dimers, further detailed AC susceptibility measurements for evaluating the relaxation parameters of **1** is not attempted in the present work.

4. Conclusion

The first cyclohexanediamine-based Mn-dimer complex, $[Mn(salcy)(N_3)]_2$ (**1**), has been isolated in diluted lacunary polyoxoanion $[PW_9O_{34}]^{9-}$ solution. Field-dependent AC susceptibility reveals that **1** shows single-molecular magnet behavior at 2–5 K. In contrast with other Schiff base ligands, salcy-based dimer complexes are rarely observed. The present work validates our synthetic strategy that POM solution possesses the template effect for Schiff base complexes. Because of the diversity of POMs, further research will focus on the introduction of different types of POMs media with distinct charge, composition, and shape and size to systematically explore the template effect for Schiff base complexes. Research on this field is underway.

Supplementary material

Crystallographic data for the structural analyses have been deposited with the Cambridge Crystallographic Data Center, CCDC reference number 1021210 and 1021209 for **1** and **2**, respectively. These data can be obtained free of charge at www.ccdc.cam.ac.uk/conts/retrieving.html (or from the Cambridge Crystallographic Data Center, 12 Union Road, Cambridge CB2 1EZ, UK; Fax:+44–1223/336–033; E-mail: deposit@ccdc.cam.ac.uk).

Funding

This work was supported by the National Natural Science Foundation of China [grant number 21201090], the Science and Technology Department of Yunnan Province Youth Project [grant number 2012FD045], and Kunming University Talent Introduction Funds [grant number YJL11028].

References

[1] A. Müller, P. Gouzerh. *Chem. Eur. J.*, **20**, 4862 (2014).
[2] R. Modak, Y. Sikdar, S. Mandal, C.J. Gómez-García, S. Benmansour, S. Chatterjee, S. Goswami. *Polyhedron*, **70**, 155 (2014).
[3] C. Ritchie, A. Ferguson, H. Nojiri, H.N. Miras, Y.-F. Song, D.-L. Long, E. Burkholder, M. Murrie, P. Kögerler, E.K. Brechin, L. Cronin. *Angew. Chem. Int. Ed.*, **47**, 5609 (2008).
[4] H. Tian, M. Wang, L. Zhao, Y.N. Guo, Y. Guo, J. Tang, Z. Liu. *Chem. Eur. J.*, **18**, 442 (2012).
[5] L.F. Zou, L. Zhao, Y.N. Guo, G.M. Yu, Y. Guo, J. Tang, Y.H. Li. *Chem. Commun.*, **47**, 8659 (2011).
[6] A. Yamashita, A. Watanabe, S. Akine, T. Nabeshima, M. Nakano, T. Yamamura, T. Kajiwara. *Angew. Chem. Int. Ed.*, **50**, 4016 (2011).
[7] N. Hoshino, A.M. Ako, A.K. Powell, H. Oshio. *Inorg. Chem.*, **48**, 3396 (2009).
[8] T. Yamaguchi, J.P. Costes, Y. Kishima, M. Kojima, Y. Sunatsuki, N. Bréfuel, J.P. Tuchagues, L. Vendier, W. Wernsdorfer. *Inorg. Chem.*, **49**, 9125 (2010).
[9] T.C. Stamatatos, G. Christou. *Inorg. Chem.*, **48**, 3308 (2009).
[10] T. Pathmalingam, S.I. Gorelsky, T.J. Burchell, A.C. Bédard, A.M. Beauchemin, R. Clérac, M. Murugesu. *Chem. Commun.*, **24**, 2782 (2008).
[11] L. Lecren, W. Wernsdorfer, Y.G. Li, A. Vindigni, H. Miyasaka, R. Clérac. *J. Am. Chem. Soc.*, **129**, 5045 (2007).
[12] H. Miyasaka, A. Saitoh, S. Abe. *Coord. Chem. Rev.*, **251**, 2622 (2007).
[13] A. Garcia-Deibe, A. Sousa, M.R. Bermejo, P.P. Mac Rory, C.A. McAuliffe, R.G. Pritchard, M. Helliwell. *Chem. Commun.*, **10**, 728 (1991).
[14] E. Gallo, E. Solari, N. Re, C. Floriani, A. Chiesi-Villa, C. Rizzoli. *J. Am. Chem. Soc.*, **119**, 5144 (1997).
[15] S. Mandal, G. Rosair, J. Ribas, D. Bandyopadhyay. *Inorg. Chim. Acta*, **362**, 2200 (2009).
[16] G. Bhargavi, M.V. Rajasekharan, J.P. Costes, J.P. Tuchagues. *Polyhedron*, **28**, 1253 (2009).
[17] S. Saha, D. Mal, S. Koner, A. Bhattacherjee, P. Gütlich, S. Mondal, M. Mukherjee, K.I. Okamoto. *Polyhedron*, **23**, 1811 (2004).
[18] H. Miyasaka, R. Clérac, W. Wernsdorfer, L. Lecren, C. Bonhomme, K.I. Sugiura, M. Yamashita. *Angew. Chem., Int. Ed.*, **43**, 2801 (2004).
[19] M.L. Wei, J.J. Sun, X.Y. Duan. *Eur. J. Inorg. Chem.*, **2014**, 345 (2014).
[20] A.-X. Yan, H.-Q. Tan, D. Liu, Z.-M. Zhang, E.-B. Wang. *Inorg. Chem. Commun.*, **29**, 49 (2013).
[21] X. Meng, C. Qin, X.L. Wang, Z.M. Su, B. Li, Q.H. Yang. *J. Chem. Soc., Dalton Trans.*, 9964 (2011).
[22] Y. Sawada, W. Kosaka, Y. Hayashi, H. Miyasaka. *Inorg. Chem.*, **51**, 4824 (2012).
[23] Q. Wu, Y.G. Li, Y.H. Wang, R. Clérac, Y. Lu, E.B. Wang. *Chem. Commun.*, **38**, 5743 (2009).
[24] Q. Wu, X. Hao, X. Feng, Y. Wang, Y. Li, E. Wang, X. Zhu, X. Pan. *Inorg. Chem. Commun.*, **22**, 137 (2012).
[25] H. Miyasaka, R. Clérac, T. Ishii, H.C. Chang, S. Kitagawa, M. Yamashita. *J. Chem. Soc., Dalton Trans.*, 1528 (2002).
[26] SAINT. Bruker AXS Inc., Madison, WI (2007).
[27] (a) G.M. Sheldrick. *Acta Crystallogr.*, **A64**, 112 (2007); (b) G.M. Sheldrick. *SADABS*, University of Göttingen, Göttingen, Germany (1996).
[28] C.P. Landee, M.M. Turnbull. *J. Coord. Chem.*, **67**, 375 (2014).
[29] J.J. Borrás-Almenar, J.M. Clemente-Juan, E. Coronado, B.S. Tsukerblat. *J. Comput. Chem.*, **22**, 985 (2001).